Short episodes of crust generation during protracted accretionary processes: evidence from Central Asian Orogenic Belt, NW China

Gong-Jian Tang[1,2], Sun-Lin Chung[3], Chris J. Hawkesworth[4, 5], P.A. Cawood[4, 6], Qiang Wang[1,2], Derek A. Wyman[7], Yi-Gang Xu[1], Zhen-Hua Zhao[1]

[1]State Key Laboratory of Isotope Geochemistry, Guangzhou Institute of Geochemistry, Chinese Academy of Sciences, Guangzhou 510640, China

[2] CAS Center for Excellence in Tibetan Plateau Earth Sciences (CETES)

[3]Department of Geosciences, National Taiwan University, Taipei, Taiwan, China

[4]Department of Earth Sciences, University of St. Andrews, North Street, St. Andrews, Fife KY16 9AL, UK.

[5]Department of Earth Sciences, University of Bristol, Wills Memorial Building, Queens Road, Bristol BS8 1RJ, UK

[6]School of Earth, Atmosphere & Environment, Monash University, Melbourne, VIC 3800, Australia

[7]School of Geosciences, The University of Sydney, NSW 2006, Australia.

*Corresponding authors:

Gong-Jian Tang

E-mail address: tanggj@gig.ac.cn (G-J, Tang); Telephone: +86 20 85290277

Abstract

Accretionary orogens are major sites of generation of continental crust but the spatial and temporal distribution of crust generation within individual orogens remains poorly constrained. Paleozoic (~540–270 Ma) granitic rocks from the Alati, Junggar and Chinese Tianshan segments of the Central Asian Orogenic Belt (CAOB) have markedly bimodal age frequency distributions with peaks of ages at ~400 Ma and 280 Ma for the Altai segment, and ~430 Ma and 300 Ma for the Junggar and Chinese Tianshan segments. Most of the magma was generated in short time intervals (~20 – 40 Ma), and variations in magma volumes and in Nd–Hf isotope ratios are taken to reflect variable rates of new crust generation within a long-lived convergent plate setting. The Junggar segment is characterised by high and uniform Nd–Hf isotope ratios (ε_{Nd}(t) = +5 – +8; zircon ε_{Hf}(t) = +10 – +16) and it appears to have formed in an intra–oceanic arc system. In the Altai and Chinese Tianshan segments, the Nd–Hf isotope ratios (ε_{Nd}(t) = -7 – +8; zircon ε_{Hf}(t) = -16 – +16) are lower, although they increase with decreasing age of the rock units. The introduction of a juvenile component into the Chinese Tianshan and Altai granitic rocks appears to have occurred in continental arc settings and it reflects a progressive reduction in the contributions from old continental lower crust and lithospheric mantle. Within the long-lived convergent margin setting (over ~200 Ma), higher volumes of magma, and greater contributions of juvenile material, were typically emplaced over short time intervals of ~20 - 40 Ma. These intervals were associated with higher Nb/La ratios, coupled with lower La/Yb ratios, in both the mafic and granitic rocks, and these episodes of increased magmatism from intraplate-like sources are therefore thought to have been in response to lithospheric extension. The trace element and Nd-Hf isotope data, in combination with estimates of granitic magma volumes, highlight that crust generation rates are strongly non-uniform within long-lived accretionary orogens. The estimated crust generation rates range from ~0.1 to ~40 km^3/km/Ma for the Paleozoic record of the CAOB, and only comparatively short (20 - 40 Ma) periods of elevated magmatic activity had rates similar to those for modern intra-oceanic and continental arcs.

Keywords: Accretionary orogen, Crustal generation, Granites, North Xinjiang, Central Asian Orogenic Belt

1. Introduction

Accretionary orogens form along convergent plate margins and they are major sites of juvenile crust production (Cawood et al., 2013, and references therein). They are complex zones with long histories of lithospheric interaction resulting in the generation of new crust, the recycling of material to the mantle through subduction erosion and sediment subduction, and of lithospheric reworking during tectonothermal events (e.g. Scholl and von Huene, 2007; Stern, 2011; Cawood et al., 2013 and references therein). There is increasing evidence that continental growth takes place in different ways in different accretionary orogens, including outward growth of juvenile magmatic arcs, and mantle input during extensional, back-arc rifting episodes (Sengör et al., 1993; Davidson and Arculus, 2006; Cawood et al., 2009; Kemp et al., 2009). In many cases the implication is that juvenile crust generation is associated with the extensional stage of accretionary orogens, whereas both crustal reworking and recycling are associated with compressional stages (Kemp et al., 2009; Collins et al., 2011).

The Central Asian Orogenic Belt (CAOB; also named the Altaids, Fig. 1a) extends from the Urals in the west, to the Okhotsk Sea along the eastern Russian coast, and it represents a major pulse of Phanerozoic continental growth (Sengör et al., 1993; Jahn, 2004; Kröner et al., 2007; Wilhem et al., 2012). This paper focuses on the Chinese Tianshan, the Junggar and the Altai segments of the North Xinjiang region, and each provides a record of igneous activity throughout most of the Paleozoic. The Chinese Tianshan segment is divided into North, Central, and South Tianshan and the Yili Block (Fig. 1c). We present a synthesis of over 2100 whole rock trace element analyses and some 860 Nd isotope and almost 4000 zircon Hf isotope analyses from granitic and mafic rocks in these temporally overlapping accretionary systems. These are combined with estimates of the outcrop areas of granitic rocks of different ages in the different segments to evaluate changes in magma volumes, and by implication provide a proxy of magma productivity. Magma productivity is highly variable during the overall history of long-lived accretionary orogens, and in this contribution we use isotope and trace element data (1) to evaluate the amount and nature of juvenile contributions to granitic magmas at different stages, and (2) to link changes in tectonic activity to crust production in the North Xinjiang segment of the CAOB. The data highlight that most of the magma, and more than 90 % of the juvenile component in the North Xinjiang segments, as evaluated from the surface areas of different granites, was emplaced over short time intervals. This has implications for crustal growth in accretionary orogens worldwide.

2. Geological background and Paleozoic magmatism

The CAOB is one of the largest accretionary orogenic belts in the world, and it encompasses an area roughly 5000 km (E–W) in length and up to 800 km (N–S) in width (Sengör et al., 1993; Windley et al., 2007; Kröner et al., 2014) (Fig. 1a). It has a long and complex tectonic evolution from at least ~ 1.0 Ga, focused in the northern part of the orogen (Khain et al., 2002), to ~ 250 Ma (Xiao et al., 2003), and associated with the growth and consumption of the Paleo-Asian Ocean. It is characterized by accretion of a number of terranes including island arcs, ophiolites, accretionary prisms, and possibly some microcontinents (Kröner et al., 2007; Windley et al., 2007). The outstanding feature of the CAOB is the vast expanse of granitic and volcanic rocks that are characterized by positive $\varepsilon_{Nd}(t)$ and young T_{DM} model ages, representing the world's largest region of continental crust generation during the Phanerozoic (Jahn, 2004). However, recent Nd-Hf isotopic data for felsic magmatic rocks have been used to argue that the volume of new crust has been grossly over estimated in the CAOB, which would not support models invoking unusually high crust generation rates during its accretionary history (Kröner et al., 2014).

The southern part of the CAOB in the North Xinjiang region of China extends about

800 km across strike, and from north to south it consists of three broadly contemporaneous accretionary assemblages: the Altai, Junggar and Chinese Tianshan segments (Fig. 1b-c). These accretionary assemblages are thought to have formed through successive subduction and accretion events along the margins of the Paleo–Asian Ocean that lay between the Siberian and Tarim cratons (Xiao et al., 2003; Wilhem et al., 2012). The Tarim Craton accreted to the Yili-Central Tianshan block on the southern margin of the CAOB, primarily in the late Carboniferous, following northward closure of the Paleo–Asian Ocean (and its branch oceans). The timing of the closure of the ocean is constrained by ca. 320 Ma suture-related eclogite overlain nonconformably by undeformed young Carboniferous limestone at Kyrgyz in the South Tianshan (Hegner et al., 2010). Consequently, post-290 Ma magmatic rocks are significantly younger than the age of accretion/collision (Kröner et al., 2014).

The Chinese segment of the Altai consists of variably deformed and metamorphosed Neoproterozoic to Paleozoic sedimentary and volcanic rocks (Sun et al., 2008). The Altai segment is separated from the Junggar segment by the Erqis suture (Fig. 1c), which contains Devonian to early Carboniferous ophiolitic rocks. Boninites, magnesian andesites, adakites, high-Ti basalts and Nb-rich basalts occur in tectonic blocks along this suture zone (Shen et al., 2014).

Voluminous Paleozoic granitic intrusions, with ages ranging from 500 Ma to 250 Ma (Fig. 2a), occur throughout the Altai segment and account for more than 40 % of the exposed rocks (Yuan et al., 2007). The granitic intrusions include metaluminous I-type, peraluminous S-type, and geochemically distinctive A-type plutons. I- and S-type intrusions were mainly emplaced in the early Paleozoic, with minor I-type intrusions emplaced in the late Paleozoic, whereas most A-type intrusions are younger and were emplaced in the early Permian (Fig. 1e). Most granitic rocks from the Altai segment are calcic and calc-alkalic (Frost et al., 2001) (Supplemental Fig. 1). The outcrop area, and by inference the volume of the granitic intrusions in the Altai segment declines with decreasing age of emplacement after the peak at about 400 Ma (Fig. 2).

The Junggar segment of the CAOB is characterized by Paleozoic ophiolitic mélanges and volcanic rocks and it is divided into eastern and western parts separated by the Junggar Basin. Geochemical and isotopic evidence are consistent with the formation of the Junggar segment in an intraoceanic arc setting (Zheng et al., 2007). The basement to the Junggar Basin consists of mainly late Paleozoic volcanic rocks with minor shales and tuffs (Zheng et al., 2007). The western Junggar region also consists of Paleozoic volcanic and sedimentary assemblages intruded by granitic rocks. No significantly older basement has been documented in the western Junggar region.

U–Pb age dating of zircon from the granitic intrusions within the Junggar segment indicate that most were emplaced during the late Carboniferous and early Permian, with a minority in the Silurian (Fig. 2a). Geochemically, these intrusions consist of

A-type and subordinate I-type granites, and most granitic rocks are calc-alkalic and alkalic-calcic (Frost et al., 2001) (Supplemental Fig. 1). In contrast to the Altai granites, the outcrop area of these Junggar granitic intrusions increases with decreasing emplacement age (Fig. 1e).

The Tianshan segment extends east-west for more than 2400 km from Uzbekistan to Xinjiang in China (Gao et al., 2009) (Fig. 1b-c). It represents an extended belt of Paleozoic magmatism that was associated with subduction beneath lithosphere containing blocks of Precambrian basement formed in the early Neoproterozoic. The Chinese Tianshan is dominated by Paleozoic S-, I- and A-type granitic intrusions, metasedimentary rocks and minor mafic rocks (Gao et al., 2009). Most of the granitic rocks are calc-alkalic and alkalic-calcic (Supplemental Fig. 1). These rock types and the geochemical characteristics of the Chinese Tianshan granitic intrusions are similar to those of the Altai segment, and they were emplaced from 500 Ma to 270 Ma, also with a bimodal distribution of ages (Figs. 1d; 2a). Most granitic intrusions were emplaced during two intervals at 310–290 Ma and 470–430 Ma (Fig. 2a), and the outcrop area of rocks associated with the younger pulse is greater than that for the older phase (Fig. 2a).

3. Age Frequency Distributions and Magma Volumes

It can be difficult to evaluate the extent to which the frequency distribution of U–Pb zircon ages reflects variations in the volumes of magmatic rocks, and hence in the rates at which magmas were generated. Figure 2a shows the frequency distribution of zircon ages for the CAOB compared with the areas of the present day exposures of granitic rocks, which are taken to be a proxy for the magma volumes, in the Altai, Junggar and Chinese Tianshan segments. It is striking how well the age frequency distributions and the variations in estimated areal extents compare; the peaks and troughs in the frequency distribution of crystallization ages are similar to the peaks and troughs of the areas of granites of different ages. All three segments have bimodal age frequency distributions with peaks of ages at ~400 Ma and 280 Ma for the Altai segment, and ~430 Ma and 300 Ma for the Junggar and Chinese Tianshan segments. Nonetheless, more than 90% of the granitic rocks in the Chinese Tianshan and the Junggar segments formed at ~300 ± 10 Ma, and at ~400 ± 20 Ma in the Altai segment, so that each segment tends to be characterised by one dominant period of magma emplacement. Overall, the estimated areas of granitic rocks, and by implication the magma volumes of the Altai segment decrease after about 400 Ma, whereas those for the Junggar segment increase with decreasing age. The variation of inferred magma volumes with age in the Chinese Tianshan segment is complex, and periods of high magma production mainly occur at about 300 Ma. The key observation is that most of the magma was generated in short time intervals (~20 – 40 Ma), and all three segments have bimodal distributions of inferred magma volumes (Fig. 2).

Figure 2b compares the age frequency distributions for granitic and mafic rocks from the Altai, Junggar and Chinese Tianshan segments. Although mafic rocks are more difficult to date, and there are many fewer ages, the age frequency distributions for the granitic and mafic rocks are very similar. Links between the present-day outcrop areas of granitic rocks and the associated magma volumes are discussed in more detail in section 5.2.

4. Secular elemental and Nd-Hf isotope variations across the Altai, Junggar and Chinese Tianshan

The geochemical data synthesized in this paper include major and trace elements analyses on 2140 samples (1360 for granitic and 780 for mafic rocks), together with 863 Nd isotope analyses, 526 U-Pb ages (427 for granitic and 99 for mafic rocks) and almost 4000 Hf isotope analyses on both magmatic (~3100) and detrital zircons (~900) (most of which had been dated previously but including more than 200 new zircon analyses) from Paleozoic igneous and sedimentary rocks in the Altai, Junggar and Chinese Tianshan segments of the CAOB (Supplemental Tables S1-4). The emphasis is on understanding the large-scale features of this belt, and the data considered are on samples from ~230 different igneous plutonic bodies and volcanic units. The approach assumes that the isotope and incompatible trace element signatures of the mafic rocks predominantly reflect their source regions in the upper mantle, whereas those of the granitic rocks predominantly reflect those of the pre-existing crust. For granites with positive $\varepsilon_{Nd}(t)$ and $\varepsilon_{Hf}(t)$ values the implication is that their crustal precursors had only recently been derived from the mantle. Such assumptions are clearly a simplification, but we would argue that they offer a realistic way forward for studies on this scale.

The variations in Nd-Hf isotope and trace elements ratios with crystallization ages for each of the segments are summarized in Table 1 and illustrated in Figure 3. The Altai, Junggar and Chinese Tianshan segments have markedly different trends of $\varepsilon_{Nd}(t)$ and $\varepsilon_{Hf}(t)$ against crystallisation age. The granitic rocks from the Junggar have high $\varepsilon_{Nd}(t)$ and $\varepsilon_{Hf}(t)$ values, ranging from +5 to +8 and from +10 to +16, respectively; these tend to be higher than those in the other segments and there is no clear change of isotope ratios with emplacement age (Fig. 3a-b). The whole rock Nd isotope ratios of the mafic rocks also display uniform and radiogenic values from +4 to +8, with no trend with emplacement age (Fig. 3c). The highly radiogenic Nd–Hf isotope compositions of the Junggar granitic rocks, and hence their young Nd-Hf model ages (500-300 Ma), are consistent with the suggestion that the basement of the Junggar Basin appears to lack Precambrian continental material. This view is further supported by the fact that less than 1% of zircon crystals analysed from this segment (10 out of 1457) yielded Precambrian U-Pb ages (Supplemental Table S4).

The Chinese Tianshan samples, in contrast to those from the Junggar Basin, show a marked increase in Nd and Hf isotope ratios with decreasing age of emplacement from 500 to 270 Ma. The average $\varepsilon_{Nd}(t)$ values increase from -4 at ~475 Ma to +4 at ~270 Ma for the Chinese Tianshan (Fig. 3a). The South Tianshan region (ie., the northern continental margin of the Tarim Craton) samples have an age frequency distribution that is strikingly bimodal, but it is unusual in that the younger samples have $\varepsilon_{Nd}(t)$ values that are markedly lower than the $\varepsilon_{Hf}(t)$ values. Thus, there is an increase in $\varepsilon_{Hf}(t)$ with decreasing emplacement age, but no similar trend for $\varepsilon_{Nd}(t)$ with age. The decoupled Nd and Hf isotopes in these younger plutons can be attributed to small degrees of source contamination by subducted pelagic sediments (Chauvel et al., 2014). The South Tianshan zircons have lower $\varepsilon_{Hf}(t)$ than most of the zircons from the Chinese Tianshan, consistent with greater contributions from older pre-existing crust. The Altai rocks exhibit a broadly similar increase in $\varepsilon_{Nd}(t)$ and $\varepsilon_{Hf}(t)$ with decreasing age, although there are fewer analyses than for the Chinese Tianshan. The whole rock Nd isotope ratios of the mafic rocks in the Chinese Tianshan and Altai segments of the CAOB also display a general trend towards higher values from ~440 Ma to 270 Ma (Fig. 3c).

Minor and trace element values reflect the tectonic setting in which the mafic magmas were generated (Pearce and Cann,1973; Kemp and Hawkesworth, 2003), and the minerals in equilibrium with the magmas, and hence the pressures and temperatures under which melt generation and crystallisation took place. Thus, depleted HREE, and associated elevated La/Yb ratios, often indicate the presence of residual garnet (Rapp and Watson, 1995) and hence that the depths of melting were greater than 30-35 km. Plagioclase is stable within continental crust, Sr is compatible in plagioclase, whereas Rb and Sm are incompatible (Severs et al., 2009). Elevated Rb/Sr ratios, and low Sr/Sm ratios, are therefore consistent with residual plagioclase and magma differentiation processes taking place within the continental crust. The Nb/La ratios of average ocean island basalts (OIB) and island arc basalts are 1.3 and 0.34, respectively (Sun and McDonough, 1989; Rudnick, 1995). High ratios (>0.71) are therefore taken to be indicative of an intraplate component, irrespective of whether that is associated with mantle plumes and/or lithospheric extension, whereas low ratios (<0.71) typically reflect magmas generated in subduction related environments. (Pearce and Peate, 1995; Condie, 1999).

Variations in selected trace element ratios with age and $\varepsilon_{Nd}(t)$ in the different mafic (SiO_2 < 53 wt.%) and granitic (SiO_2 > 56 wt.%) rock suites as summarized in Figures 4-6. Some of the trace element ratios are sensitive to the degree of (shallow level) fractionation (e.g. Rb/Sr and Sr/Sm), and some ratios change little with increasing silica (Nb/La and La/Yb). Thus for the granitic rocks, whole rock analyses are plotted for each sample and these are then compared with the same element ratios projected to 70% SiO_2 along within-suite differentiation trends, where those can be established, so that element ratios can also be compared at similar degrees of differentiation (Figs. 5-6).

Sr/Sm decreases steadily with decreasing emplacement age in the Chinese Tianshan granitic rocks, most markedly for the early Permian A-type granites, which have distinct low Sr/Sm ratios (Fig. 5). The Junggar late Carboniferous granites extend to lower Sr/Sm values and a greater range in Sr/Sm ratios relative to those of the Silurian samples (Fig. 5). In contrast, the Sr/Sm ratios increase with decreasing emplacement age for the Altai granitic rocks except for early Permian A-type granites that have distinctly low Sr/Sm ratios (Fig. 5). The Rb/Sr ratios of the granitic rocks from these three segments tend to show reverse trends to those of Sr/Sm, and the extent to which these trends reflect different degrees of differentiation in different granite bodies can be seen by comparing the changes in measured Sr/Sm and Rb/Sr with those projected to 70% SiO_2 (Fig. 5).

The variation of La/Yb with age in the granitic rocks of the Chinese Tianshan segment is complex (Fig. 5) (Table 1). In samples older than ~290 Ma, La/Yb ratios generally decrease with decreasing age, but they then increase in the early Permian rocks with decreasing emplacement age. In the Junggar segment, the late Carboniferous granitic rocks have lower values, but a greater range of La/Yb ratios than the Silurian samples, and the La/Yb ratios of the Altai granitic rocks increase with decreasing emplacement age (Fig. 5). The Nb/La ratios also show more complex variations. For the Chinese Tianshan and Junggar segments, late Paleozoic (~300 ± 10 Ma) granites have high and larger ranges of Nb/La ratios, whereas in the Altai segment the early Paleozoic samples (400 ± 20 Ma) have the higher Nb/La ratios and exhibit a greater range.

In the plots of trace element ratios with $\varepsilon_{Nd}(t)$ for the granitic rocks (Fig. 6), samples from the Junggar segment have a limited range of $\varepsilon_{Nd}(t)$ and no correlations are observed with trace element ratios. In the Altai segment, the low $\varepsilon_{Nd}(t)$ values are linked to low Sr/Sm and high Rb/Sr ratios for both the raw data and the values projected to 70% SiO_2. This is consistent with models in which the crustal material sampled in the more differentiated magmas is characterised by relatively old model, or source, ages. In contrast, in the Chinese Tianshan segment it is the rocks with high $\varepsilon_{Nd}(t)$ values that tend to be associated with low Sr/Sm and high Rb/Sr ratios, and the changes with $\varepsilon_{Nd}(t)$ are more marked for the raw data than for the data projected to 70% SiO_2 (Fig. 6). In this case the more differentiated magmas have sampled crustal source rocks with relatively young model ages. The Nb/La and La/Yb ratios do not correlate with $\varepsilon_{Nd}(t)$ values in any of the three segments.

Figures 7 summarises variations in Nb/La, La/Yb and $\varepsilon_{Hf}(t)$ with age and with the surface areas of the different granites, which is taken to be a proxy for the magma volumes of the magmatic rocks of different ages in the three areas. It highlights that there is relatively little systematic change in Nb/La in the Altai rocks, a slight increase in Nb/La with increasing magma volumes in the Chinese Tianshan, and a range in Nb/La in the Junggar rocks that increase with both decreasing magmatic age and increasing magma volumes. For La/Yb, there are similar systematic changes in all three segments, with a slight decrease in La/Yb with increasing magma volumes. There are no clear changes in Sr/Sm and Rb/Sr with magma volumes (not shown) except that average Rb/Sr increases from ~0.1 to 10 with increasing magma volumes in the Junggar, consistent with the observation that the periods of high magma volumes are marked by relatively high silica granitic rocks. There is little variation in $\varepsilon_{Hf}(t)$ in the Junggar rocks and no correlation was observed with magma volumes. In contrast, a slight decrease occurs in $\varepsilon_{Hf}(t)$ with increasing magma volumes in the Altai, and a more marked increase in $\varepsilon_{Hf}(t)$ with magma volumes in the Chinese Tianshan (Fig. 7).

5. Discussion

The topics considered are (i) the implications of crustal thickness and tectonic setting on the observed isotope and trace element changes with time (Figs. 3-7), (ii) the causes of the variations in the volumes of magma emplaced at different times, and (iii) the wider topic of crust generation in accretionary orogens. To summarize, the age frequency distributions of the mafic and granitic rocks are similar (Fig. 2b), and the isotope and trace element ratios of the mafic rocks can be used to evaluate the nature of mantle derived magmas and how they changed with time (Figs. 4 and 7). However, the magmatic record in the CAOB is dominated by granitic rock types and so only those rock types are used to evaluate magma volumes, and the volumes of new crust generated.

5.1 Isotope and trace element changes with time

The strongly radiogenic Nd and Hf isotope ratios of the mafic and granitic rocks of the Junggar segment are consistent with magma sources set in a juvenile intra-oceanic arc. In contrast, granites in the Chinese Tianshan and Altai segments have relatively low Nd and Hf isotope ratios ($\varepsilon_{Nd}(t)$ and zircon $\varepsilon_{Hf}(t)$ are as low as -7 and -16, respectively.) that imply contributions from older, and more isotopically unradiogenic basement rocks in these areas.

The REE's patterns of subduction related lavas may be related to the thickness of the crust in which they occur (Kay and Kay, 2002). Elevated La/Yb ratios and, in particular, low HREE are consistent with the presence of garnet, and hence indicate the depths of melting and/or fractional crystallisation. Alternative mechanisms for increasing La/Yb ratios in granitic magmas, such as monazite fractionation, are not viable for the granites studied here (see Supplemental Figure 2). The increasing La/Yb, and decreasing Yb contents, of the Altai granitic rocks with decreasing emplacement age suggests that the depth of crustal melting increased with time, indicating that the crust of the Altai segment may have thickened through the history of accretion (Figs. 4-5). However, samples with lower ε_{Nd} tend also to have lower Sr/Sm and higher Rb/Sr ratios (Fig. 6), suggesting that the lower ε_{Nd} values are associated with relatively shallow level trace element signatures within the crust. In contrast, the granitic rocks of the Chinese Tianshan segment exhibit trends of decreasing La/Yb with decreasing age before 290 Ma and then increasing La/Yb subsequently, consistent with shifts to shallower levels of melting before 290 Ma and then to deeper levels thereafter (Fig. 5). Sr/Sm tends to be lower and Rb/Sr to be higher in the rocks with higher ε_{Nd} values (Fig. 6), implying that the higher ε_{Nd} values ($\varepsilon_{Nd}(t) > +4$) are associated with more middle to upper crustal mineral assemblages.

In each area the Nb/La ratios of the mafic and granitic rocks exhibit broadly similar patterns in rocks of different ages (Fig. 7). The mafic rocks of the Junggar segment are characterised by simple variations from low to high Nb/La ratios, from more arc-type to more intraplate-like magmas, with decreasing age (Fig. 4). The associated granitic rocks have a similar pattern displaced to higher Nb/La values with decreasing age (Fig. 5). In contrast, the Nb/La ratios of the mafic and the granitic rocks of the Chinese Tianshan and Altai segments are broadly similar and they show no systematic change with emplacement age. The Junggar rocks show little variation in Nd isotopic compositions, but in the Chinese Tianshan Nb/La tends to be lower in the rocks with higher ε_{Nd}, consistent with more mantle material being emplaced in a subduction related settings. However, in the Altai, the rocks with higher ε_{Nd} exhibit a significant range in Nb/La indicating contributions from both intraplate and subduction-modified mantle in the generation of these magmas.

5.2 Intermittent magmatic activity

Accretionary orogens typically evolve over ca. 200–300 Ma (Condie, 2007; Cawood et al., 2009), and yet the Tianshan, Junggar and Altai segments have markedly bimodal age frequency distributions with two zircon age peaks spanning ~20–40 Ma punctuated by age troughs that can be up to 150 Ma in duration (Fig. 2a).

Geochemically, the periods of relatively high magma volumes are characterised by elevated Nb/La ratios, and these are associated with lower La/Yb in the Junggar segment, to a lesser extent in the Chinese Tianshan, and they are perhaps very slightly coupled in the Altai (Fig.7). The mafic rocks, including dikes, intrusive plutons and volcanic rocks, which are widely distributed in North Xinjiang during phases of extensive magmatism, display dual or hybrid arc and MORB like geochemical characteristics. In contrast, the mafic rocks formed during periods of low magma volumes show island arc characteristics (Cai et al., 2010; Tang et al., 2012). The high values and larger range of Nb/La, and the low La/Yb ratios of the mafic rocks generated in periods of relatively high volumes of magma are consistent with the involvement of an intraplate-like asthenospheric mantle component, which likely signifies mantle upwelling to relatively shallow levels during lithospheric extension.

Field relations and geochemical evidence provide further support for extensional settings during phases of high volumes of magmatism. For example, these phases of magma emplacement are characterized by i) development of intra-arc basins characterized by bimodal volcanic rocks that formed by rising asthenosphere caused the rifting of the overriding plate in an extensional setting (Shen et al., 2014), ii) widely distributed mafic and intermediate dikes also suggest an extensional setting during the time of their formation (Tang et al., 2012), and iii) voluminous A-type granites, especially in the Junggar and Tianshan segments (Fig. 1d-e), which are emplaced in an extensional setting coupled with mantle upwelling (Tang et al., 2012). More widely, Collins et al. (2011) noted that in what they termed external orogenic systems, such as those around the Pacific rim, the range in Hf isotope ratios narrowed and trended towards more radiogenic values through time. This is similar to the trends recognised here (Fig. 3) and Collins et al. (2011) attributed such features to the progressive removal of lower crust and lithospheric mantle by continuing subduction. However, they found no evidence that a greater intraplate signature developed through time, and in that sense the CAOB data are different in that the trends to more positive Hf and Nd isotope ratios are consistent with an increased intraplate component in periods of increased magma volumes. Our results show that the mafic magmas contemporaneous with the granites range up to OIB-like compositions during the periods of high volumes of magmatism. The mafic magmas are most plausibly attributed to extensional crustal episodes and the sporadic high-volume magmatism interspersed with lower volume background magmatism is consistent with this scenario.

Overall, the CAOB magmatic rocks were generated in response to southward accretion from the southern active margin of the Siberian Craton to final closure of the Paleo-Asian ocean when the Tarim and North China cratons were attached to the CAOB (Xiao et al., 2003; Windley et al., 2007; Wilhem et al., 2012). The peri-Siberian region, which constitutes the northern part of the CAOB, developed by multiple accretion–collision events around the microcontinents of Tuva-Mongolia and Altai-Mongolia by the end of the early Paleozoic (Wilhem et al., 2012). Subsequently, new subduction systems tended to occur in the Altai region in the central part of the CAOB along the new Siberian margin and largely from the Silurian to early Devonian (Yuan et al., 2007). Most of the magmatic rocks of the Junggar and Chinese Tianshan regions in the southern part of the CAOB were then generated in the late Carboniferous (Fig. 2). Thus, magma pulses tended to be younger from the north to the south, consistent with southward accretion of the CAOB. The feature of intermittent magmatic activity is a feature of the whole CAOB, and it is not just restricted to the north Xinjiang (Xiao et al., 2003; Windley et al., 2007; Wilhem et al., 2012).

5.3 Non-uniform crustal addition

Granitic rocks dominate the magmatic record preserved in the CAOB, and they are closer in composition to the bulk continental crust. The discussion of the amounts of magma generated and of new continental crust formed therefore focuses on the granitic rocks. To estimate the juvenile contributions to the magmas over time, the juvenile end-member was taken to be mafic rocks coeval with the different granitic rocks (Supplemental Table S5), and the crustal end-member was felsic with the integral crustal Hf isotope ratio (Fig. 3) and 5.3 ppm Hf (Rudnick and Gao, 2003). Two component mixing calculations indicate that the juvenile input to the granitic magmatism varied from ~ 68 % to almost 98 % for Altai and from ~ 60 % to ~ 95 % in the Chinese Tianshan (Fig. 8a). Such figures are very generalised, but they give a sense of the overall changes. Jahn (2004) reached similar conclusions, estimating a 60–100 % juvenile component in CAOB granitic rocks based on the Nd isotope compositions.

As indicated above, areas of outcrop can be taken as proxies of magma volumes, and we now address in more detail what the volumes of magma might represent. Based on a global compilation of volumetric volcanic output rates (White et al., 2006), we assume an intrusive to extrusive ratio of 5:1 to estimate the volume of the volcanic rock, and an average thickness of granite of 15 ± 10 km. The North Xinjiang contains less Precambrian basement compared with other areas of the CAOB. Thus, for the whole CAOB, it remains more difficult to constrain the volumes of new crust than in the North Xinjiang (Kröner et al., 2014).

The estimated crust generation rates for the Chinese Tianshan, Junggar and Altai segments are presented in Figure 8b. They are based on the lengths for each of the arc segments of approximately 400, 200 and 280 km, respectively (Fig. 8a). The average rates of crust generation for the three segments show strong temporal variations, ranging from ~0.1 to ~40 km^3/km/Ma (volume per unit width along the strike direction of the arc) (Fig. 8b). Such figures are significantly lower than the high rates of crust generation proposed for the North Xinjiang region in the CAOB of ~230 km^3/km/Ma from ~550 Ma to 260 Ma (Condie, 2007) and critically they highlight the variable magma generation rates through time. Comparison of these rates of magma generation with those from recent destructive plate margins of 40-180 and 75-100 km^3/km/Ma for intra-oceanic arcs and for periods of magma flare-up in North American continental arcs respectively (Holbrook et al., 1999; Jicha et al., 2006; Nikolaeva et al., 2008) further highlights that in the CAOB the maximal rates of magma generation were only close to overall global averaged rates of crust generation in the relatively short periods of high magmatic activity. Moreover, such agreement with the magma volumes in more recent systems offers support for the assumptions made to convert areas of granite into magma volumes (Fig. 8b).

The results from the CAOB emphasise that nearly all the new crust formed in relatively short intervals (~20-40 Ma), albeit at different times in different segments. For example, the most significant period of new crust formation for the Altai segment occurred at ~400 ± 20 Ma. Early Permian (ca. 290-270 Ma) A-type granites in the Altai are characterized by depleted Nd–Hf isotopic compositions, but they have a small outcrop area indicating only minor crustal growth during that time. The high rate of new crust formation at ~300 ± 10 Ma for the Junggar and Chinese Tianshan segments is associated with A and I-type magmatism. Figure 8b shows that juvenile crust generation in the North Xinjiang segments was highly variable, although the zircon Hf isotopic ratios of granitic rocks increases with decreasing emplacement age. More specifically, more than 90 % of new juvenile crust was added in a short interval (20–40 Ma) during the overall long-lived ~200 Ma of accretionary processes (Fig. 8).

5.4 *Implications for crust generation in accretionary orogens*

Non-uniform magmatic productivity and crust generation may be an intrinsic feature of individual accretionary orogens and it has been reported from the Arabian–Nubian Shield (Robinson et al., 2014), the east Australian segment of the Terra Australis orogen (Collins, 2002; Kemp et al., 2009), the North American Cordillera (Ducea et al., 2015), and the modern Aleutians (Jicha et al., 2006).

The correspondence of the magmatic lull in the Altai segment with high magmatic activity in the Chinese Tianshan and Junggar suggests linked kinematics for the geometry of the plate convergent systems of the Paleo-Asian Ocean (Fig. 2a). Whether these links reflect regional drivers specific to the CAOB or are driven by far field effects is difficult to evaluate given the inherently incomplete nature of the rock and plate kinematic record. We note however, that the timing of late Paleozoic events in the CAOB is contemporaneous with a number of events associated with the final assembly of Pangea, both within the interior of the supercontinent associated with closure of the Rheic Ocean and around the periphery of the supercontinent along its paleo-Pacific margin (Cawood and Buchan, 2007).

On a global scale detrital zircon Hf-O isotopic data sets suggest that new continental crust has been generated continuously through time, with a progressive decrease in the rate of crustal growth since the Archean, in part due to the increased volumes of crust recycled through subduction zones (Dhuime et al., 2012). A significant amount of new crust was generated in Phanerozoic accretionary orogens, and the CAOB is a prime example given that it is characterized by significant juvenile crustal production (Sengör et al., 1993; Jahn, 2004; Kröner et al., 2007), similar to the circum–Pacific accretionary orogens (Cawood et al., 2009; Collins et al., 2011). Furthermore, the overall continuous rate of crustal growth implies that local variations in individual orogens are linked via the global plate kinematic framework with regions of low growth buffered by regions of high growth.

Summary

i) Most magmatism (> 90%) is concentrated into relatively short time periods between 540-270 Ma, which for the Chinese Tianshan and Junggar segments is ~300 ± 10 Ma, and for the Altai segment is ~400 ± 20 Ma. Thus, each segment tends to be characterised by one dominant period of magma emplacement.

ii) The variations in Nd and Hf isotope ratios are different in the three segments. In the Chinese Tianshan and Altai the Nd and Hf isotope ratios increase to increasingly mantle−like values in the younger rocks ($\varepsilon_{Nd}(t)$ = -7 – +8; zircon $\varepsilon_{Hf}(t)$ = -16 – +16), in contrast to the Junggar segment that is characterised by high and uniform Nd–Hf isotope ratios throughout ($\varepsilon_{Nd}(t)$ = +5 – +8; zircon $\varepsilon_{Hf}(t)$ = +10 – +16).

iii) The periods of high magma volumes tend to be associated with higher Nb/La ratios coupled with lower La/Yb ratios, albeit to different degrees in the different segments. The higher Nb/La values are attributed to an increased contribution of intraplate magmatism, which may reasonably be linked to an increased role of extensional tectonics in the periods of increased magma volumes.

iv) Most of the juvenile crust added during the Paleozoic was restricted to relatively short time periods when the magma generation rates were similar to those along modern subduction zones. Estimated average rates of crust generation for the three segments show strong temporal variations, ranging from ~0.1 to ~40 km^3/km/Ma, and the maximal rates of magma generation were only close to overall global averaged rates of crust generation in the relatively short periods of high magmatic activity.

Acknowledgments

We thank Editor-in-Chief Professor An Yin, Professors Alfred Kröner, Scott Samson and two anonymous reviewers for their constructive and helpful reviews on the manuscript. This study was supported by funding from the Strategic Priority Research Program (B) of the Chinese Academy of Sciences (grant no. XDB03010600 and XDB18020204), the National Natural Science Foundation of China (grant nos. 41202041 and 41673033), and GIG–CAS 135 project Y234021001. PAC and CJH acknowledge support from the Natural Environment Research Council (grant NE/J021822/1). The senior author thanks the grant from the NSC, Taiwan, which supported his one-year academic visit at the NTU. This is contribution no. XXXXXX from GIG–CAS.

References

Belousova, E.A., Kostitsyn, Y.A., Griffin, W.L., Begg, G.C., O'Reilly, S.Y., Pearson, N.J., 2010. The growth of the continental crust: Constraints from zircon Hf-isotope data. Lithos 119, 457-466.

Cawood, P.A., Buchan, C., 2007. Linking accretionary orogenesis with supercontinent assembly. Earth-Science Reviews 82, 217-256.

Cawood, P.A., Hawkesworth, C.J., Dhuime, B., 2013. The continental record and the generation of continental crust. Geol Soc Am Bull 125, 14-32.

Cawood, P.A., Kroner, A., Collins, W.J., Kusky, T.M., Mooney, W.D., Windley, B.F., 2009. Accretionary orogens through Earth history. Geological Society, London, Special Publications 318, 1-36.

Cai, K., Sun, M., Yuan, C., Zhao, G., Xiao, W., Long, X., Wu, F., 2010. Geochronological and geochemical study of mafic dykes from the northwest Chinese Altai: Implications for petrogenesis and tectonic evolution. Gondwana Res 18, 638-652.

Chauvel, C., Garçon, M., Bureau, S., Besnault, A., Jahn, B.M., Ding, Z., 2014. Constraints from loess on the Hf–Nd isotopic composition of the upper continental crust. Earth Planet Sci Lett 388, 48-58.

Collins, W.J., Belousova, E.A., Kemp, A.I.S., Murphy, J.B., 2011. Two contrasting Phanerozoic orogenic systems revealed by hafnium isotope data. Nature Geosci 4, 333-337.

Condie, K.C., 1999. Mafic crustal xenoliths and the origin of the lower continental crust. Lithos 46, 95-101.

Condie, K.C., 2007. Accretionary orogens in space and time. Geological Society of America Memoirs 200, 145-158.

Davidson, J.P., Arculus, R.J., 2006. The significance of Phanerozoic arc magmatism in generating continental crust., in: Brown, M., Rushmer, T. (Eds.), Evolution and Differentiation of the Continental Crust. Cambridge University Press, pp. 135-172.

Dhuime, B., Hawkesworth, C.J., Cawood, P.A., Storey, C.D., 2012. A Change in the Geodynamics of Continental Growth 3 Billion Years Ago. Science 335, 1334-1336.

Ducea, M.N., Saleeby, J.B., Bergantz, G., 2015. The Architecture, Chemistry, and Evolution of Continental Magmatic Arcs. Annu Rev Earth Plant Sci. 43, 299-331.

Frost, B.R., Barnes, C.G., Collins, W.J., Arculus, R.J., Ellis, D.J., Frost, C.D., 2001. A Geochemical Classification for Granitic Rocks. J Petrol 42, 2033-2048.

Gao, J., Long, L., Klemd, R., Qian, Q., Liu, D., Xiong, X., Su, W., Liu, W., Wang, Y., Yang, F., 2009. Tectonic evolution of the South Tianshan orogen and adjacent regions, NW China: geochemical and age constraints of granitoid rocks. Int J Earth Sci 98, 1221-1238.

Griffin, W.L., Pearson, N.J., Belousova, E., Jackson, S.E., van Achterbergh, E., O'Reilly, S.Y., Shee, S.R., 2000. The Hf isotope composition of cratonic mantle: LAM-MC-ICPMS analysis of zircon megacrysts in kimberlites. Geochim Cosmochim Acta 64, 133-147.

Hegner, E., Klemd, R., Kröner, A., Corsini, M., Alexeiev, D.V., Iaccheri, L.M., Zack, T., Dulski, P., Xia, X., Windley, B.F., 2010. Mineral ages and P-T conditions of Late Paleozoic high-pressure eclogite and provenance of mélange sediments from Atbashi in the south Tianshan orogen of Kyrgyzstan. Am J Sci 310, 916-950.

Jahn, B.M., 2004. The Central Asian Orogenic Belt and growth of the continental crust in the Phanerozoic, in: Malpas, J., Fletcher, C.J.N., Ali, J.R., Aichison, J.C. (Eds.), Aspects of the Tectonic Evolution of China. Geological Society, London, Special Publications, London, pp. 73-100.

Jicha, B.R., Scholl, D.W., Singer, B.S., Yogodzinski, G.M., Kay, S.M., 2006. Revised age of Aleutian Island Arc formation implies high rate of magma production. Geology 34, 661-664.

Kay, R.W., Kay, S.M., 2002. Andean adakites: three ways to make them. Acta Petrologica Sinica 18, 303-311.

Kemp, A.I.S., Hawkesworth, C.J., 2003. Granitic Perspectives on the Generation and Secular Evolution of the Continental Crust, in: Heinrich, D.H., Karl, K.T. (Eds.), Treatise on Geochemistry. Pergamon, Oxford, pp. 349-410.

Kemp, A.I.S., Hawkesworth, C.J., Collins, W.J., Gray, C.M., Blevin, P.L., 2009. Isotopic evidence for rapid continental growth in an extensional accretionary orogen: The Tasmanides, eastern Australia. Earth Planet Sci Lett 284, 455-466.

Khain, E.V., Bibikova, E.V., Kroner, A., Zhuravlev, D.Z., Sklyarov, E.V., Fedotova, A.A., Kravchenko-Berezhnoy, I.R., 2002. The most ancient ophiolite of the Central Asian fold belt: U-Pb and Pb-Pb zircon ages for the Dunzhugur Complex, Eastern Sayan, Siberia, and geodynamic implications. Earth Planet Sci Lett 199, 311-325.

Kröner, A., Kovach, V., Belousova, E., Hegner, E., Armstrong, R., Dolgopolova, A., Seltmann, R., Alexeiev, D.V., Hoffmann, J.E., Wong, J., Sun, M., Cai, K., Wang, T., Tong, Y., Wilde, S.A., Degtyarev, K.E., Rytsk, E., 2014. Reassessment of continental growth during the accretionary history of the Central Asian Orogenic Belt. Gondwana Res 25, 103-125.

Kröner, A., Windley, B.F., Badarch, G., Tomurtogoo, O., Hegner, E., Jahn, B.M., Gruschka, S., Khain, E.V., Demoux, A., Wingate, M.T.D., 2007. Accretionary growth and crust formation in the Central Asian Orogenic Belt and comparison with the Arabian-Nubian shield, in: Hatcher, R.D., Jr, Carlson, M.P., McBride, J.H. (Eds.), A 4-D framework of continental crust. Geological Society of America Memoirs, pp. 181-209.

Nikolaeva, K., Gerya, T.V., Connolly, J.A.D., 2008. Numerical modelling of crustal growth in intraoceanic volcanic arcs. Phys Earth Planet In 171, 336-356.

Pearce, J.A., Cann, J.R., 1973. Tectonic setting of basic volcanic rocks determined using trace element analyses. Earth Planet. Sci. Lett. 19(2), 290–300.

Pearce, J.A., Peate, D.W., 1995. Tectonic Implications of the Composition of Volcanic arc Magmas. Annu Rev Earth Plant Sci. 23, 251-285.

Rapp, R.P., Watson, E.B., 1995. Dehydration Melting of Metabasalt at 8-32 kbar: Implications for Continental Growth and Crust-Mantle Recycling. J Petrol 36, 891-931.

Robinson, F.A., Foden, J.D., Collins, A.S., Payne, J.L., 2014. Arabian Shield magmatic cycles and their relationship with Gondwana assembly: Insights from zircon U–Pb and Hf isotopes. Earth Planet Sci Lett 408, 207-225.

Rudnick, R.L., 1995. Making continental crust. Nature 378, 573–578.

Scholl, D.W., von Huene, R., 2007. Crustal recycling at modern subduction zones applied to the past,ÄîIssues of growth and preservation of continental basement crust, mantle geochemistry, and supercontinent reconstruction. Geological Society of America Memoirs 200, 9-32.

Sengör, A.M.C., Natal'in, B.A., Burtman, V.S., 1993. Evolution of the Altaid tectonic collage and Palaeozoic crustal growth in Eurasia. Nature 364, 299-307.

Severs, M.J., Beard, J.S., Fedele, L., Hanchar, J.M., Mutchler, S.R., Bodnar, R.J., 2009. Partitioning behavior of trace elements between dacitic melt and plagioclase, orthopyroxene, and clinopyroxene based on laser ablation ICPMS analysis of silicate melt inclusions. Geochim Cosmochim Acta 73, 2123-2141.

Shen, X.M., Zhang, H.X., Wang, Q., Ma, L., Yang, Y.H., 2014. Early Silurian (~440Ma) adakitic, andesitic and Nb-enriched basaltic lavas in the southern Altay Range, Northern Xinjiang (western China): Slab melting and implications for crustal growth in the Central Asian Orogenic Belt. Lithos 206–207, 234-251.

Tang, G.J., Wang, Q., Wyman, D.A., Li, Z.X., Zhao, Z.H., Yang, Y.H., 2012. Late Carboniferous high $\varepsilon_{Nd}(t)$–$\varepsilon_{Hf}(t)$ granitoids, enclaves and dikes in western Junggar, NW China: Ridge-subduction-related magmatism and crustal growth. Lithos 140–141, 86-102.

Stern, C.R., 2011. Subduction erosion: Rates, mechanisms, and its role in arc magmatism and the evolution of the continental crust and mantle. Gondwana Res 20, 284-308.

Steven Holbrook, W., Lizarralde, D., McGeary, S., Bangs, N., Diebold, J., 1999. Structure and composition of the Aleutian island arc and implications for continental crustal growth. Geology 27, 31-34.

Sun, M., Yuan, C., Xiao, W. J., Long, X. P., Xia, X. P., Zhao, G. C., Lin, S. F., Wu, F. Y., and Kroner, A., 2008. Zircon U-Pb and Hf isotopic study of gneissic rocks from the Chinese Altai: Progressive accretionary history in the early to middle Palaeozoic: Chem.Geol 247(3-4): 352-383.

Sun, S.S., McDonough, W.F., 1989. Chemical and isotopic systematics of oceanic basalts: implications for mantle composition and processes, in: Saunders, A.D., Norry, M.J. (Eds.), Magmatism in the Ocean Basins. Geological Society London Special Publications, pp. 313–345.

Vogt, K., Gerya, T.V., Castro, A., 2012. Crustal growth at active continental margins: Numerical modeling. Phys Earth Planet In 192–193, 1-20.

White, S.M., Crisp, J.A., Spera, F.J., 2006. Long-term volumetric eruption rates and magma budgets. Geochemistry, Geophysics, Geosystems 7, Q03010.

Wilhem, C., Windley, B.F., Stampfli, G.M., 2012. The Altaids of Central Asia: A tectonic and evolutionary innovative review. Earth-Science Reviews 113, 303-341.

Windley, B.F., Alexeiev, D., Xiao, W., Kroner, A., Badarch, G., 2007. Tectonic models for accretion of the Central Asian Orogenic Belt. J Geol Soc London 164, 31-47.

Xiao, W.J., Windley, B.F., Hao, J., Zhai, M.G., 2003. Accretion leading to collision and the Permian Solonker suture, Inner Mongolia, China: Termination of the central Asian orogenic belt. Tectonics 22, 1069, doi:1010.1029/2002TC001484.

Yuan, C., Sun, M., Xiao, W.J., Li, X.H., Chen, H.L., Lin, S.F., Xia, X.P., Long, X.P., 2007. Accretionary orogenesis of the Chinese Altai: Insights from Paleozoic granitoids. Chem Geol 242, 22-39.

Zheng, J.P., Sun, M., Zhao, G.C., Robinson, P.T., Wang, F.Z., 2007. Elemental and Sr-Nd-Pb isotopic geochemistry of Late Paleozoic volcanic rocks beneath the Junggar basin, NW China: Implications for the formation and evolution of the basin basement. J Asian Earth Sci 29, 778-794.

Figure captions

Fig. 1. (a) simplified tectonic divisions of the CAOB (after Jahn, 2004), showing the location of the North Xinjiang and adjact areas; (b) Digital topography of North Xinjiang and adjact area of the sourhern Central Asian Orogenic Belt (original data from U.S. Geological Survey [http://eros.usgs.gov/products/elevation/gtopo30.html]) showing the Altai, Junggar and Tianshan segments from northeast to southwest. (c) Geological map of Northern Xinjiang and adjact areas (Gao et al., 2009). NTAC- Northern Tianshan Accretionary Complex, KYB - Kazakhstan–Yili block, CTA - Central Tianshan Arc. (d-e) The outcrop area of granitic rocks of the North Xinjiang different orogens.

Fig. 2. (a) Histogram of zircon U–Pb ages for granitic rocks of the Altai, Junggar and Chinese Tianshan segments. the relative age probability (red curve) of detrital zircons from the Chinese Tianshan segment is shown for comparison. The outcrop areas of the granitic rocks are compared for every 20 Ma time intervals. The bands of high rates of magmatism based on the areas of granitic rocks in Figure 1d-e. Grey and brown bars represent age peak and period of high rate magmatism. (b) Comparion diagrams of the age frequency distributions for granitic and mafic rocks from the Altai, Junggar and Chinese Tianshan segments. Data sources are detailed in the text.

Fig. 3. Whole rock Nd and Zircon Hf isotopic values of granitic rocks (SiO_2 > 56 wt.%) from the Altai, Junggar and Chinese Tianshan segments (a, b). Whole rock $\varepsilon_{Nd}(t)$ isotopic values ratios of the mafic rocks (SiO_2 < 53 wt.%) from the the Altai, Junggar and Chinese Tianshan segments plotted as a function of crystallization ages (c). Integral crust curves in (b) represent the Hf composition of the local crust basement calculated using the method described in Belousova et al. (2010). These curves represent the average Hf isotope composition of the local continental crust at time *t*, estimated from all the zircons that crystallized before time *t*, using the average $^{176}Lu/^{177}Hf$ of the continental crust (0.0125) (Belousova et al., 2010; Chauvel et al.,

2014). The method was applied to all zircon Hf isotope data from both detrital and magmatic samples for the Chinese Tianshan and Altai segments. It is similar to, but perhaps more realistic than the crust model age calculation with interpolation projected forward in time instead of backwards. Thus it takes account of all pre-existing material, and provides an average crustal isotope value at any time (Belousova et al., 2010). The stippled blue line at 270 Ma denotes the end time of accretionarly processes in the North Xinjiang. For convenience the Chinese Tianshan orogenic system has been divided into the Tianshan segment that includes the North and Central Tianshan and Yili block, and the Southern Tianshan (Fig. 1c). The global depleted mantle value was used as the juvenile end-member, with $^{176}Hf/^{177}Hf$ at the present day of 0.28325 (Griffin et al., 2000). DM–depleted mantle, CHUR–chondritic cniform ceservoir. Data sources are detailed in the text.

Fig. 4. The North Xinjiang mafic rocks (SiO_2 < 53 wt.%) La/Yb and Nb/La ratios versus crystallization age. The end-members of the average OIB and the arc basalt are from Sun and McDonough (1989) and Rudnick (1995), respectively. Symbols for average trace element data for 20 Ma year periods are shown with black outlines. Grey and brown bars are the same as in Figure 2.

Fig. 5. Trace elements ratios versus crystallization age of granitic rocks of the North Xinjiang orogens. Large circles are raw data of the granitic rocks from the Tianshan (blue), Junggar (yellowgreen) and Altai (red) segments. Small green squares are refined data of the granitic rocks for the three segments. For the Sr/Sm and Rb/Sr ratios, all the raw data were projected to 70% SiO_2 based on within-suite differentiation trends. For the Nb/La and La/Yb ratios, only those granitic rocks with >56% SiO_2 < 66% were plotted in order to eliminate crystallization effect. Magenta triangles are raw data of the granitic rocks from the Chinese South Tianshan. The best fit lines on these plots are calculated by linear regression. Grey and brown bars are the same as in Figure 2.

Fig. 6. Selected trace element ratios versus $\varepsilon_{Nd}(t)$ isotopic values of granitic rocks of the North Xinjiang orogens. The best fit lines on these plots are calculated by linear regression. Symbols are the same as in Figure 5.

Fig. 7. The Nb/La ratios in the mafic and the granitic rocks of the Chinese Tianshan, Junggar and Altai segments for each time period (a-c); and the mafic and granitic rocks Nb/La ratios (d-f), granitic rocks La/Yb ratios (g-i) and zircon $\varepsilon_{Hf}(t)$ values (j-l) versus the outcrop area occupied by the granitic rocks of the three segments. Trace element data are presented as averages for every 20 Ma years. Grey and brown bars are the same as in Figure 2.

Fig. 8. (a) Juvenile input for Chinese Tianshan and Altai segments calculated from the zircon Hf isotope data, compared with the average $\varepsilon_{Hf}(t)$ values for granitic rocks shown by broken lines; (b) Estimated rates of crust generation (km^3/km/Ma) through time for the Chinese Tianshan, Junggar and Altai segments, adopting an average granite crustal thickness of 15 ± 10 km (error bars). For the Junggar segments, all the granitic rocks have depleted mantle like Nd-Hf isotope ratios, and so the outcrop area of the granitic rocks is taken to represent the volume of new crust. The rates for intra-oceanic arcs of Izu-Bonin, Marianas, Tonga, New Hebrides, Marianas, Southern and Northern Izu-Bonin, and Aleutian island arcs (Steven Holbrook et al., 1999; Jicha et al., 2006), and continental arc, are also compared. All calculations are presented for 20 Ma time intervals.

Table caption

Table 1. The Nd-Hf isotopic ratios, trace elements ratios variation with age of granitic rocks for each of the segments.

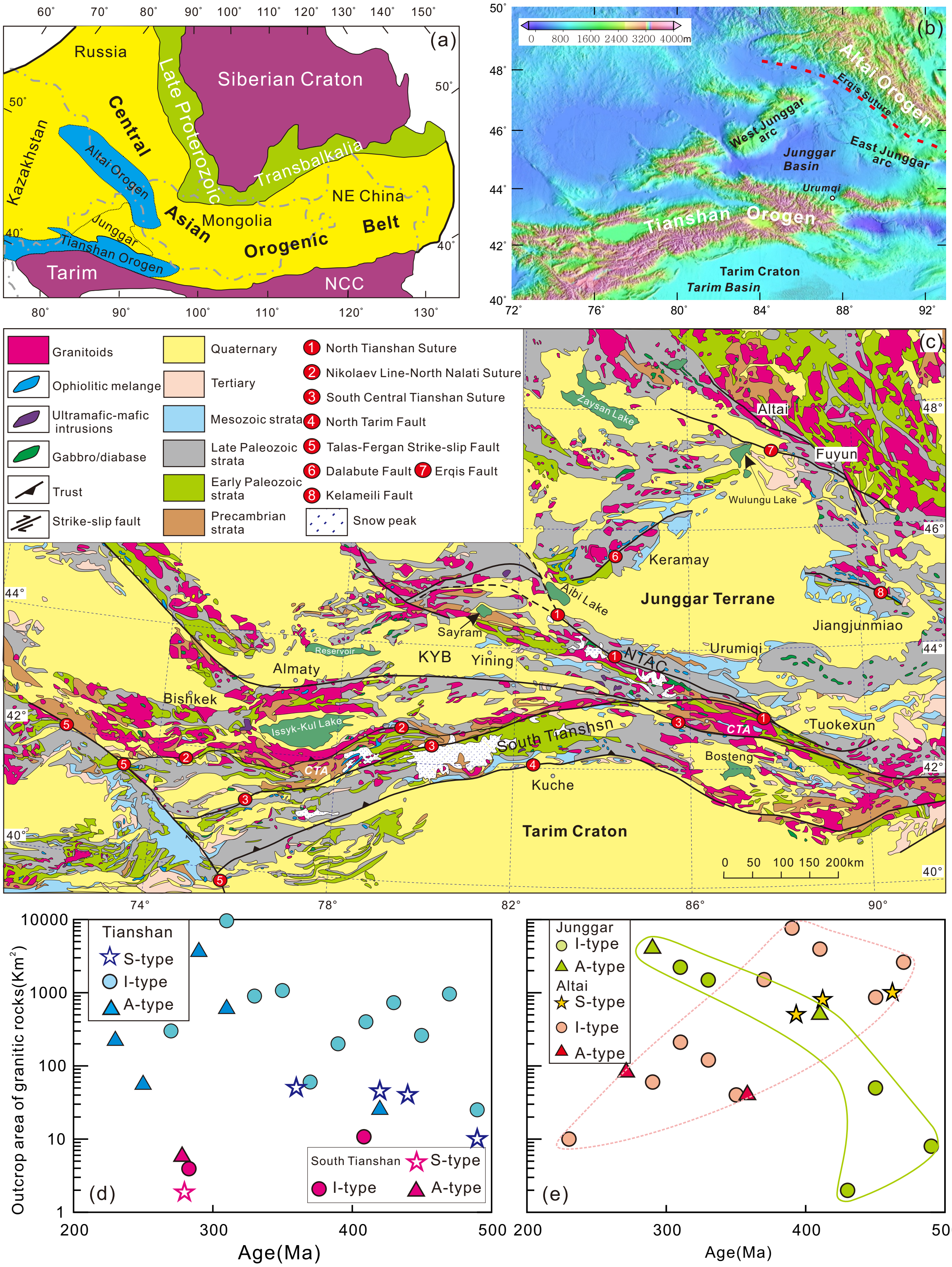
(a)
Russia
Siberian Craton
Kazakhstan
Central
Late Proterozoic
Altai Orogen
Transbalkalia
NE China
Junggar
Asian
Mongolia
Belt
Orogenic
Tianshan Orogen
Tarim
NCC
(b)
Altai Orogen
Erqis Suture
West Junggar arc
East Junggar arc
Junggar Basin
Urumqi
Tianshan Orogen
Tarim Craton
Tarim Basin
(c)
Granitoids
Ophiolitic melange
Ultramafic-mafic intrusions
Gabbro/diabase
Trust
Strike-slip fault
Quaternary
Tertiary
Mesozoic strata
Late Paleozoic strata
Early Paleozoic strata
Precambrian strata
1 North Tianshan Suture
2 Nikolaev Line-North Nalati Suture
3 South Central Tianshan Suture
4 North Tarim Fault
5 Talas-Fergan Strike-slip Fault
6 Dalabute Fault
7 Erqis Fault
8 Kelameili Fault
Snow peak
Altai
Fuyun
Zaysan Lake
Wulungu Lake
Keramay
Junggar Terrane
Aibi Lake
Jiangjunmiao
Sayram
Urumiqi
KYB
Yining
NTAC
Almaty
Bishkek
Issyk-Kul Lake
CTA
South Tianshsn
Tuokexun
Bosteng
Kuche
Tarim Craton
0 50 100 150 200km
(d)
Tianshan
S-type
I-type
A-type
South Tianshan
Outcrop area of granitic rocks(Km2)
Age(Ma)
(e)
Junggar
I-type
A-type
Altai
S-type
I-type
A-type
Age(Ma)

Figure-1

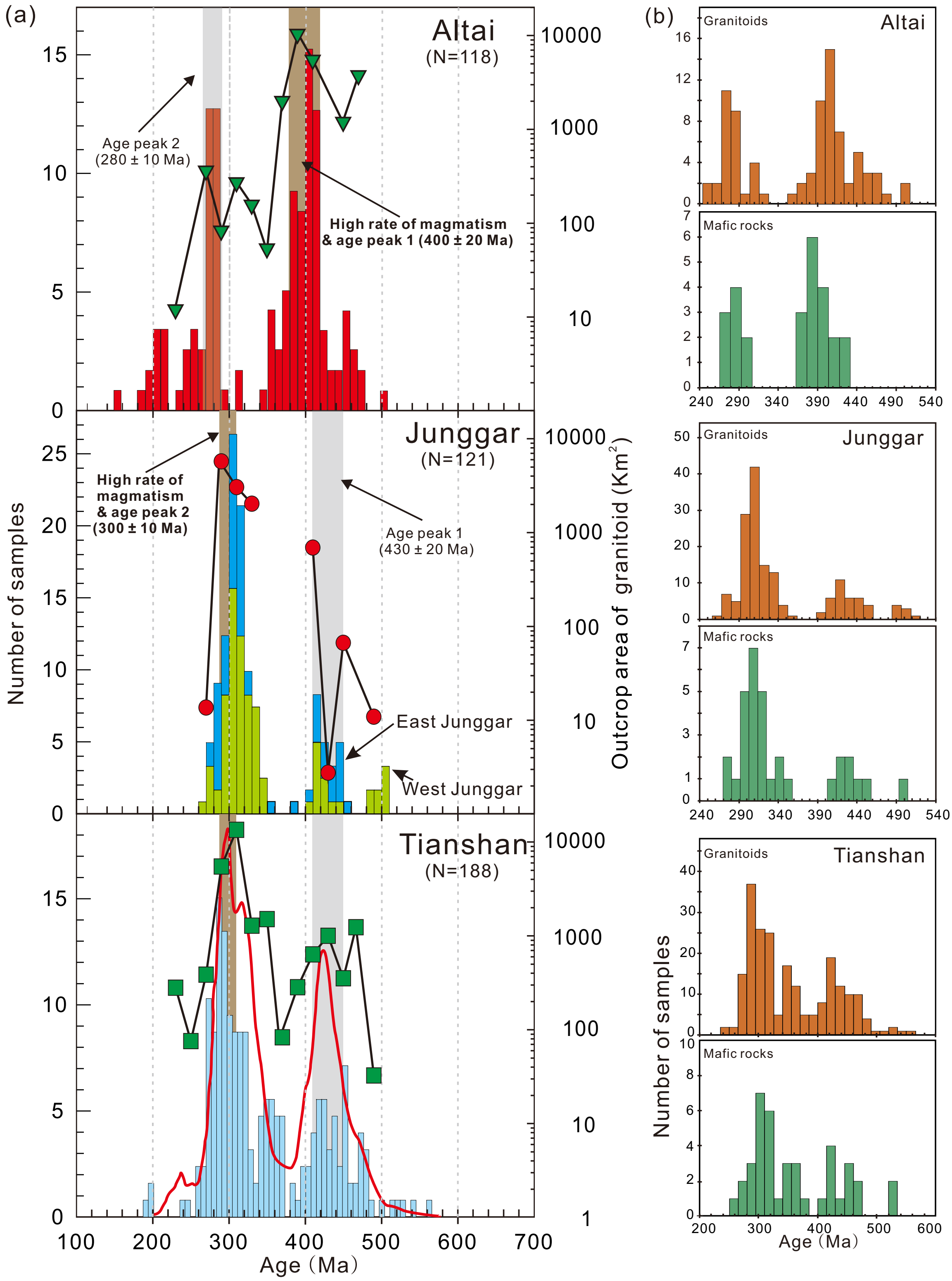

(a)
Altai
(N=118)
Age peak 2
(280 ± 10 Ma)
High rate of magmatism
& age peak 1 (400 ± 20 Ma)
Junggar
(N=121)
High rate of
magmatism
& age peak 2
(300 ± 10 Ma)
Age peak 1
(430 ± 20 Ma)
East Junggar
West Junggar
Tianshan
(N=188)
Number of samples
Outcrop area of granitoid (Km2)
Age (Ma)
(b)
Granitoids
Altai
Mafic rocks
Granitoids
Junggar
Mafic rocks
Granitoids
Tianshan
Mafic rocks
Number of samples
Age (Ma)

Figure-2

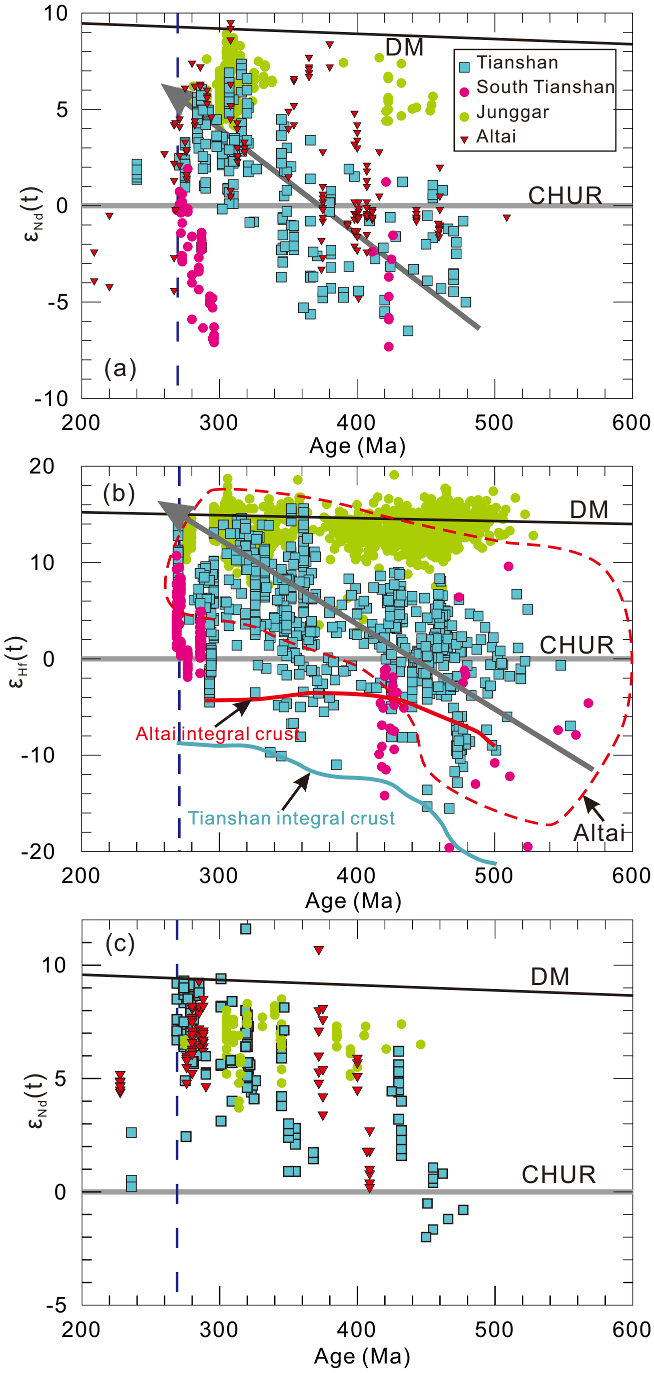

Tianshan
South Tianshan
Junggar
Altai
DM
CHUR
(a)
$\varepsilon_{Nd}(t)$
Age (Ma)
(b)
$\varepsilon_{Hf}(t)$
Altai integral crust
Tianshan integral crust
Altai
(c)

Figure-3

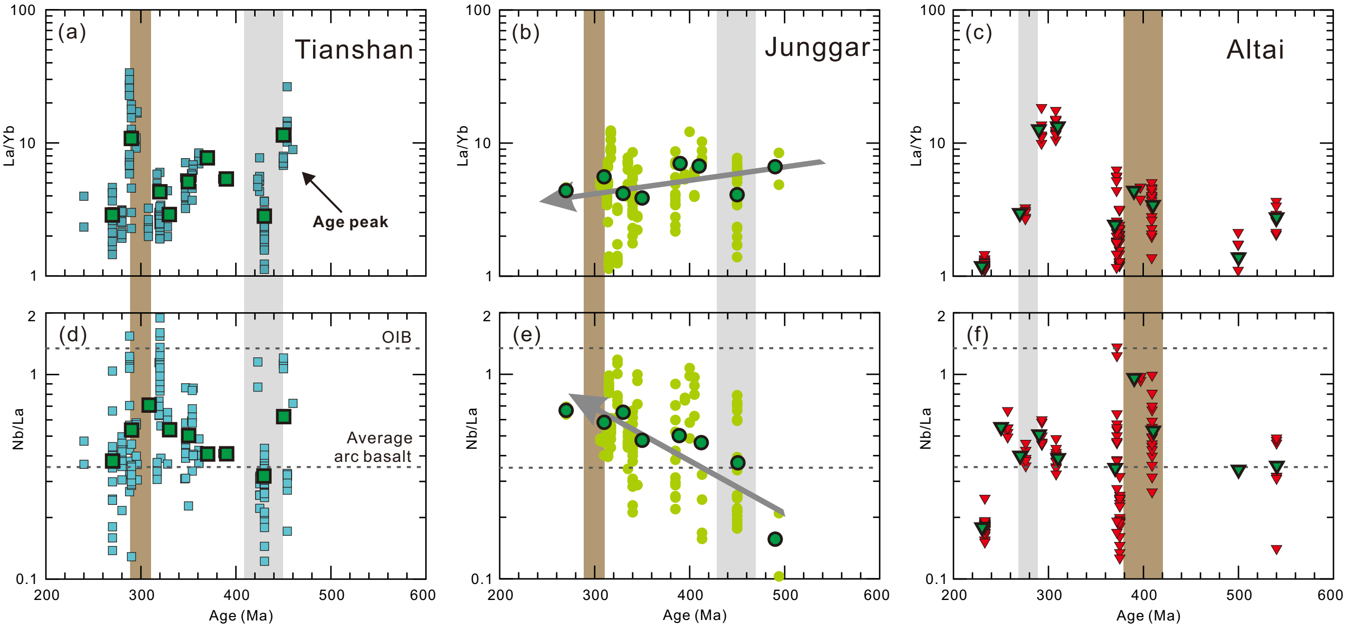
(a)
Tianshan
La/Yb
Age peak
(b)
Junggar
(c)
Altai
(d)
OIB
Average
arc basalt
Nb/La
(e)
(f)
Age (Ma)

Figure-4

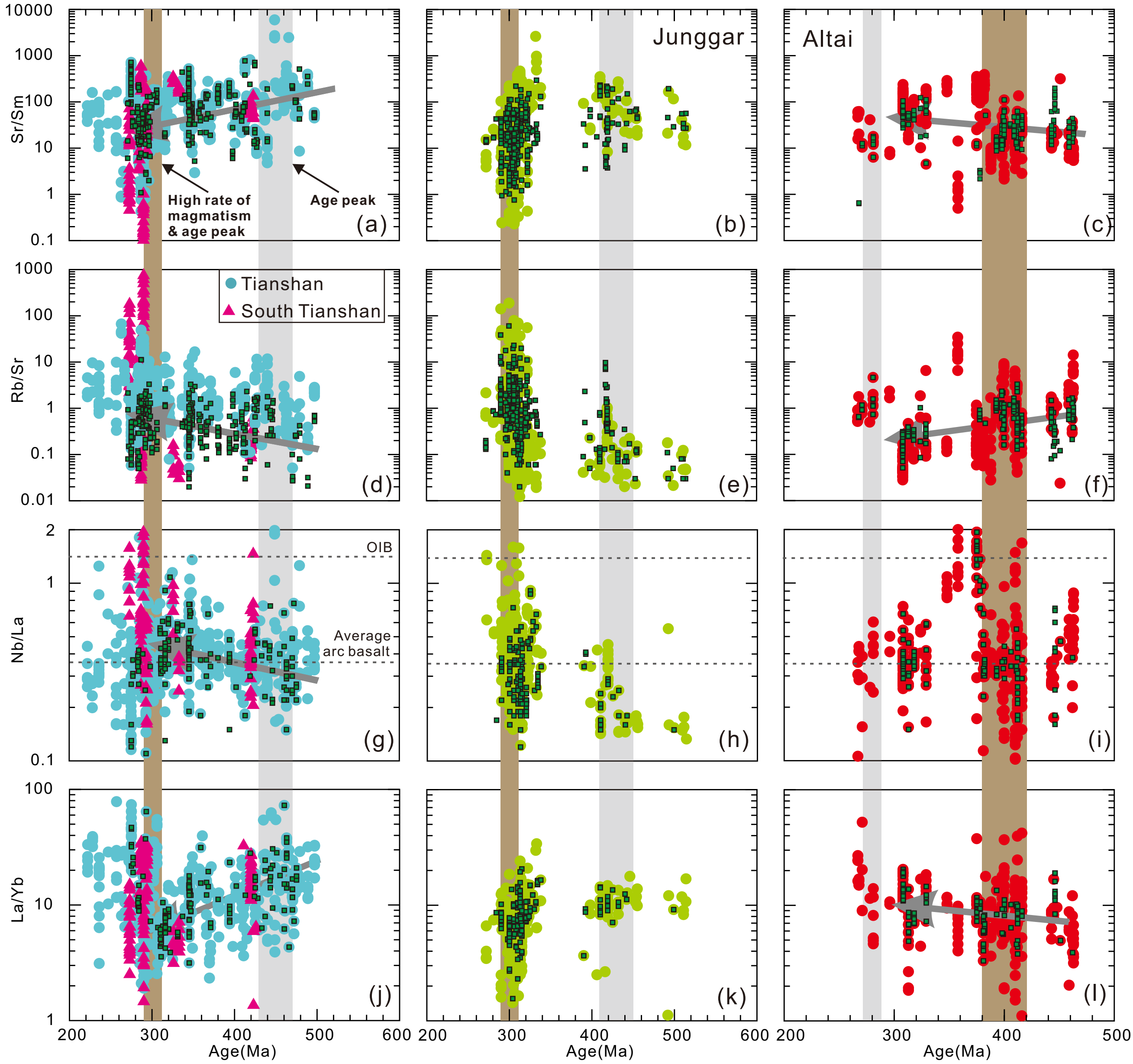

Junggar
Altai
Sr/Sm
Rb/Sr
Nb/La
La/Yb
Age(Ma)
High rate of magmatism & age peak
Age peak
Tianshan
South Tianshan
OIB
Average arc basalt
(a)
(b)
(c)
(d)
(e)
(f)
(g)
(h)
(i)
(j)
(k)
(l)

Figure-5

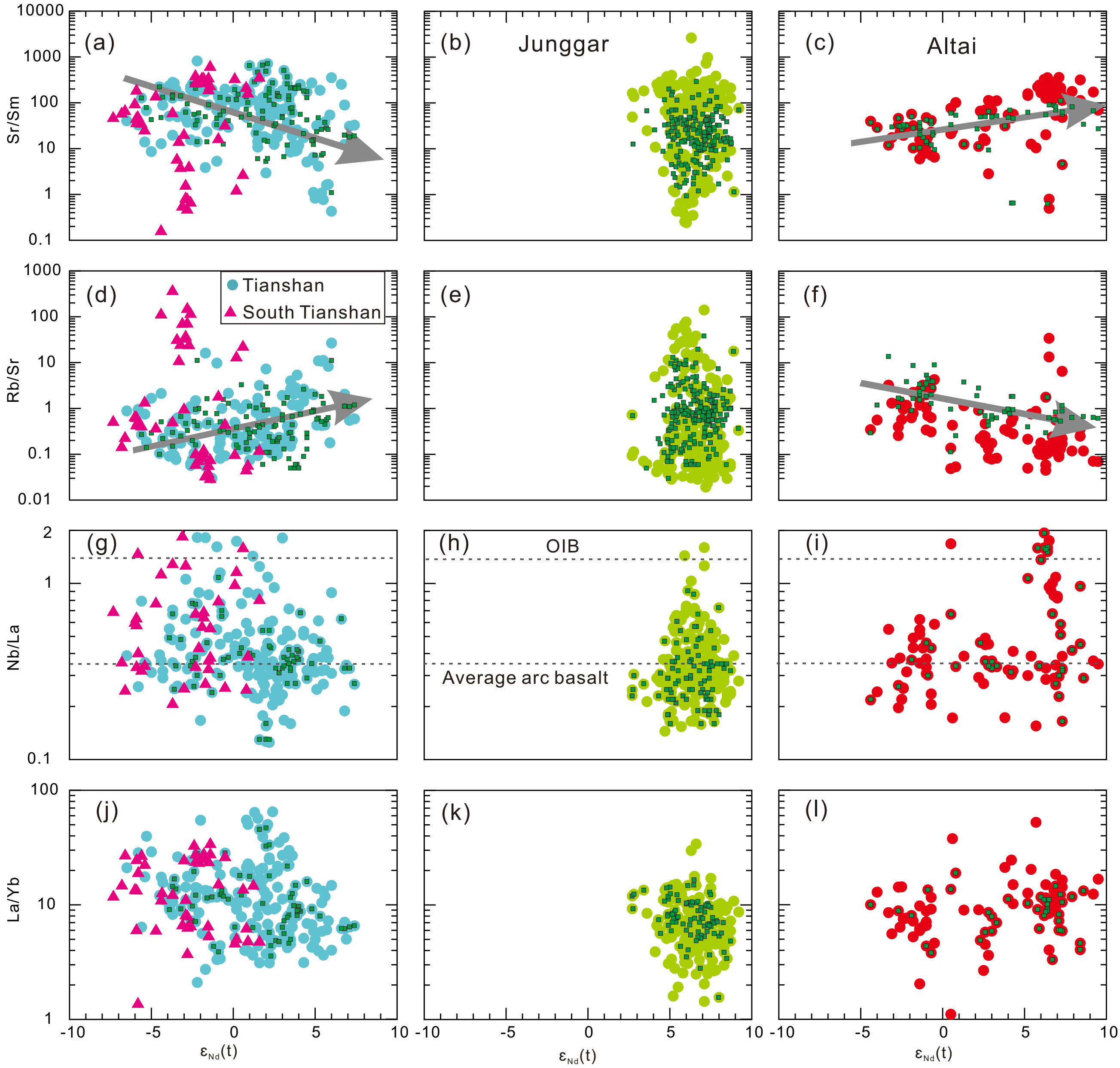

Sr/Sm
Rb/Sr
Nb/La
La/Yb
(a)
(b)
Junggar
(c)
Altai
(d)
Tianshan
South Tianshan
(e)
(f)
(g)
(h)
OIB
Average arc basalt
(i)
(j)
(k)
(l)
$\varepsilon_{Nd}(t)$

Figure-6

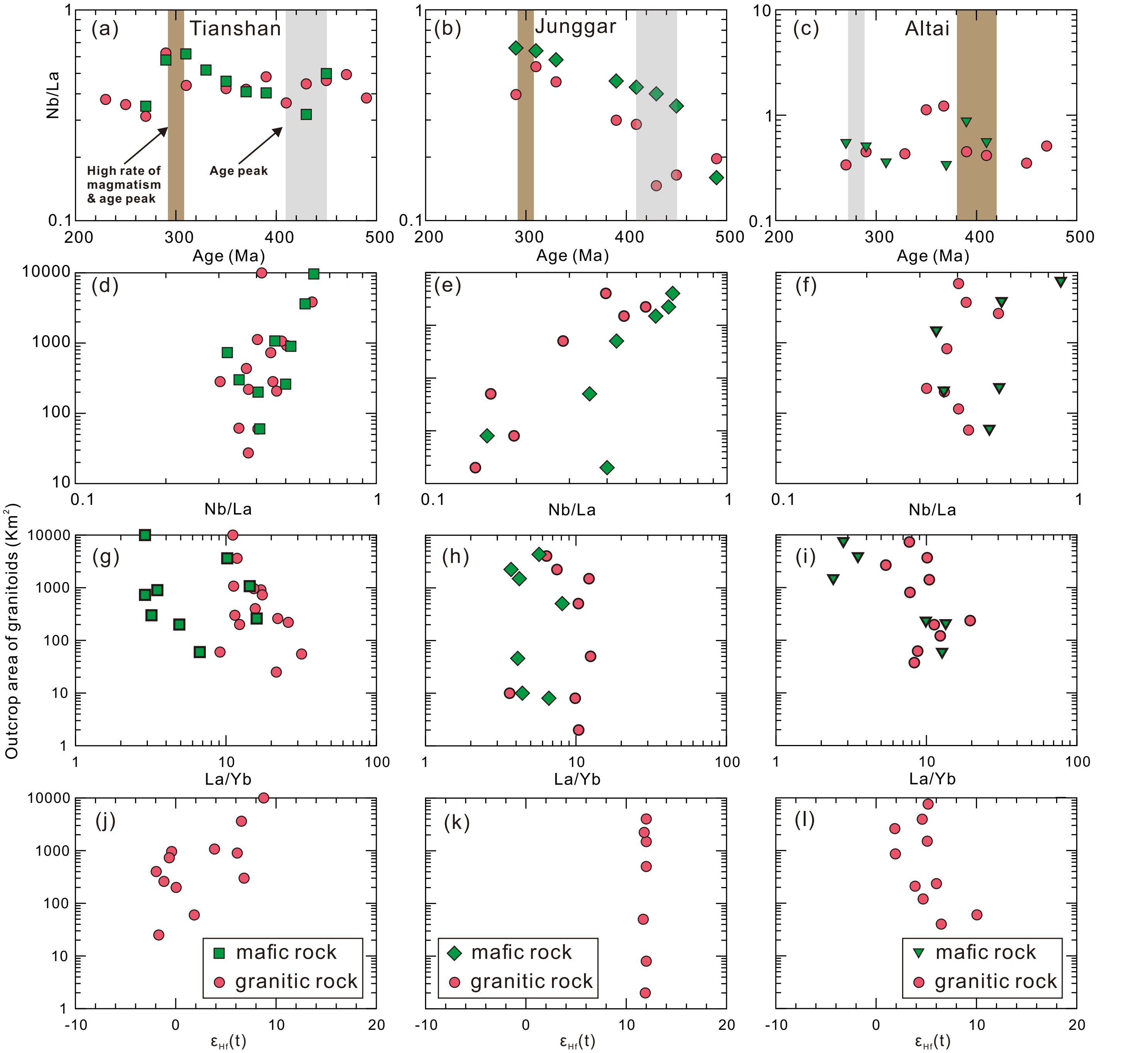

(a) Tianshan
(b) Junggar
(c) Altai
Nb/La
Age (Ma)
High rate of magmatism & age peak
Age peak
(d)
(e)
(f)
(g)
(h)
(i)
(j)
(k)
(l)
Outcrop area of granitoids (Km^2)
La/Yb
$\varepsilon_{Hf}(t)$
mafic rock
granitic rock

Figure-7

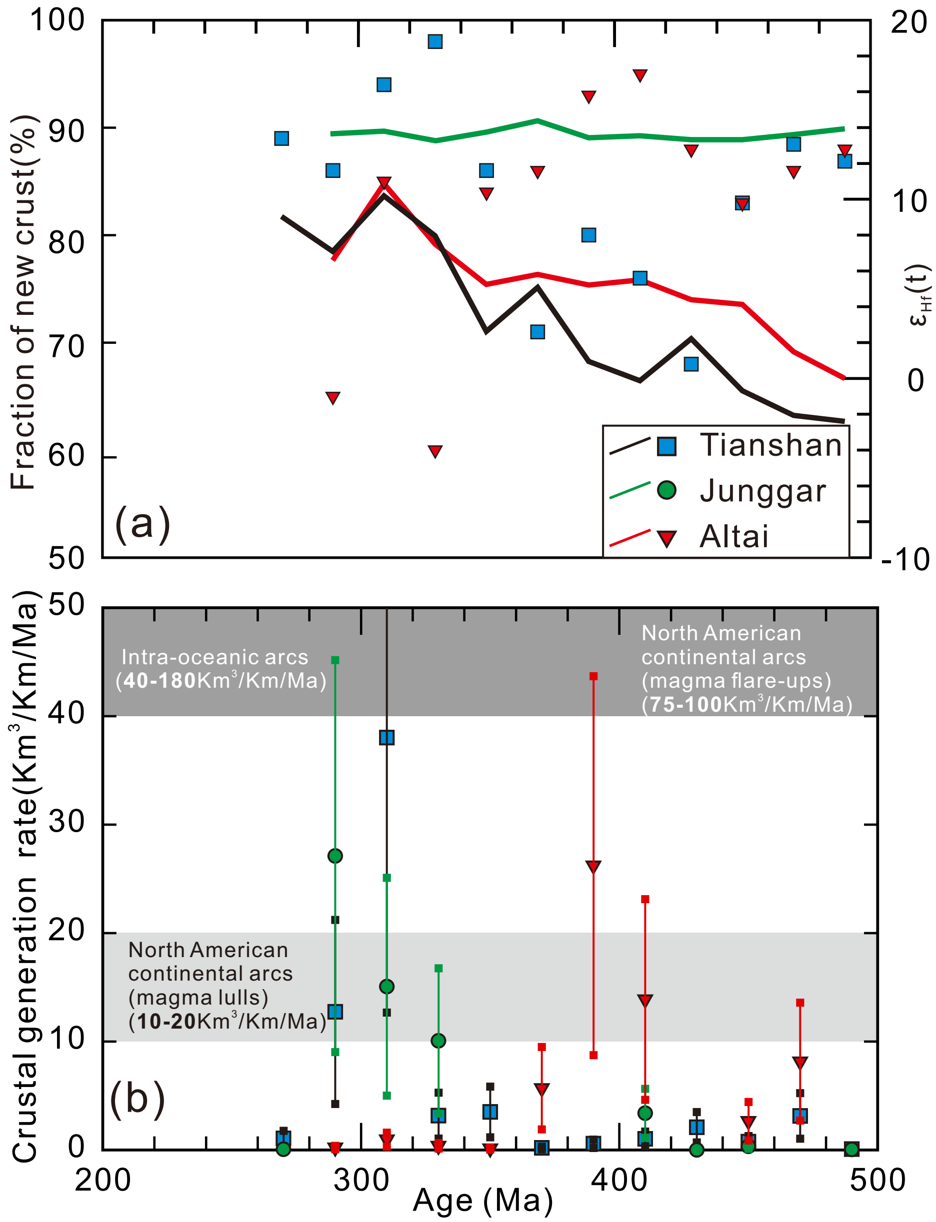

Fraction of new crust(%)
εHf(t)
Tianshan
Junggar
Altai
(a)
Crustal generation rate(Km3/Km/Ma)
Intra-oceanic arcs
(40-180Km3/Km/Ma)
North American
continental arcs
(magma flare-ups)
(75-100Km3/Km/Ma)
North American
continental arcs
(magma lulls)
(10-20Km3/Km/Ma)
(b)
Age (Ma)

Figure-8

Table 1. The Nd-Hf isotopic ratios, trace elements ratios variation of granitic rocks with age for each of the segments.

	Chinese Tianshan	Junggar	Altai
$\varepsilon_{Nd}(t)$ & $\varepsilon_{Hf}(t)$	Increase with decreasing age ($\varepsilon_{Nd}(t)$ = -7 – +7; zircon $\varepsilon_{Hf}(t)$ = -16 – +15)	High and uniform, close to the depleted mantle ($\varepsilon_{Nd}(t)$ = +5 – +8; zircon $\varepsilon_{Hf}(t)$ = +10 – +16)	Increase with decreasing age ($\varepsilon_{Nd}(t)$ = -5 – +8; zircon $\varepsilon_{Hf}(t)$ = -16 – +16)
Nb/La	Increase with decreasing age until about 290 Ma ranging from 0.4 to 0.8, high and large range at 300 ± 10 Ma (0.6 ± 0.6)	Increase with decreasing age (0.2 – *0.5*), high and large range during 300 ± 10 Ma (0.46 ± 0.2)	no systematic change (0.3 – *0.8*), but increased and large range during 400 ± 20 Ma (0.5 ± 0.4)
La/Yb	Decrease with decreasing age until about 290 Ma ranging from 8.7 to 32, lowest at 300 ± 10 Ma (8.7 ± 10)	Always low (6.4 – *12.2*), low and large range during 300 ± 10 Ma (6.9 ± 2.9),	Increase with decreasing age (5.4 – *19.8*), but always low (<20)
High rates of magmatism	300 ± 10 Ma	300 ± 10 Ma	400 ± 20 Ma
General interpretation	Crustal thinning with decreasing age until about 290 Ma and thickening after it	Crust always thin, but thinnest at 300 ± 10 Ma	Crustal thickening with decreasing age